

Chapter 3

Results

[WIP]

This thesis focuses on the impact of an inertia value at a specific network location on the oscillatory behavior of the rest of a power system. In particular, I show that the idea of localization can be used to describe the relevant oscillatory behaviors that occur for small power fluctuations. For each tested network location I quantify the transition from localized to delocalized dynamics. I then explain how this transition depends on the network location of the VRG using a new measure. These results better describe the relationship between the network location of a VRG and the inertial support it can provide. This information can be used to help narrow a possibly large search space of placement and sizing of VRG inertial support.

To begin, I show how the energetic responses of power system components change as a VRG inertia value changes. I then describe how these changes relate to the concept of localization. I then explore how the energetic responses of the system change when the perturbation dynamics are altered which does[] For each tested scenario, I show how to identify and quantify the transition from localized to delocalized dynamics using the oscillatory behavior of the system state vector. Finally, I explain the concept of dynamic sensitivity and introduce a new measure that quantifies how easy it is for oscillations to spread from the VRG to other nodes in the network. I then show that this new measure helps explain the relationship between the localization transition and the network location of a VRG.

Recall from Section 2.2.4 that the term *scenario* indicates the set of experiments conducted

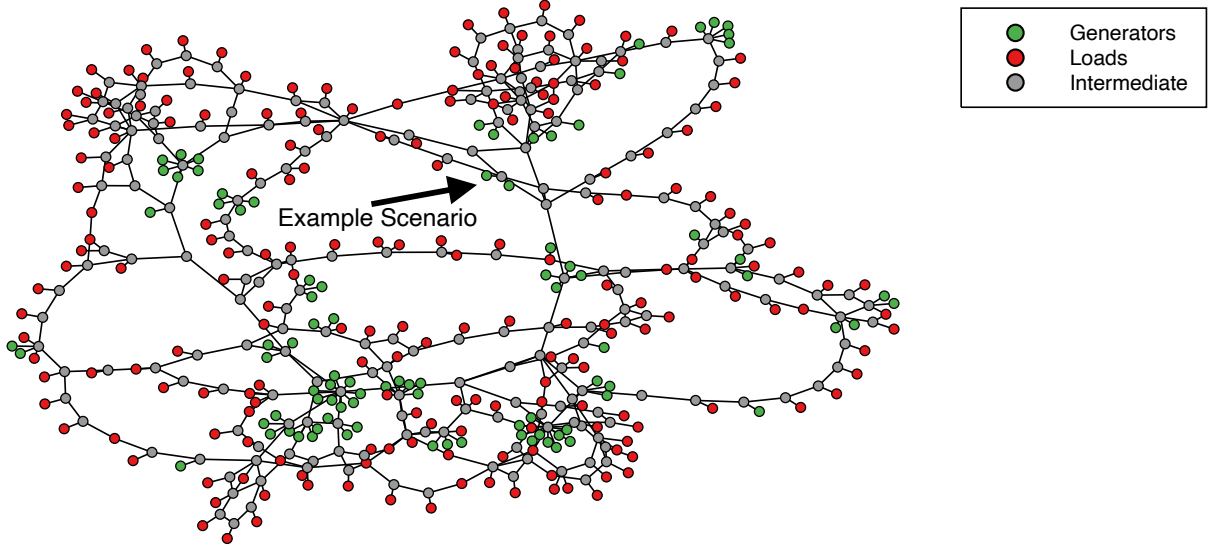


Figure 3.1: The power system used in this thesis [citation]. Green nodes indicate generators and red nodes indicate loads. The arrow points to the VRG location for the example scenario.

by delivering a perturbation to a single network location, varying the inertia value at that location, and examining the response at all other nodes and links in the network (see Section 2.2.4 for further experimental details). Additionally, the term “VRG” refers to the perturbed generator with changing inertia constant for a given scenario.

3.1 Example of Results for a Single Scenario

When there is a perturbation to the power generation of a VRG, its inertia value plays a significant role in the dynamical response of other components in the network. In this Section I describe some of the characteristics of these responses for a single scenario which are common among all of the scenarios. The VRG location for the example scenario is indicated in Figure 3.1.

Recall from Section 2.2.4 that I measure the RMS of the component energies (kinetic and nodal potential) to quantify the component response. I focus on the energies of SGs and loads as these are the only components in the network that contribute to the aforementioned energies (see Section 2.1.1). Figure 3.2 shows the energetic responses of SGs and loads for the kinetic and nodal

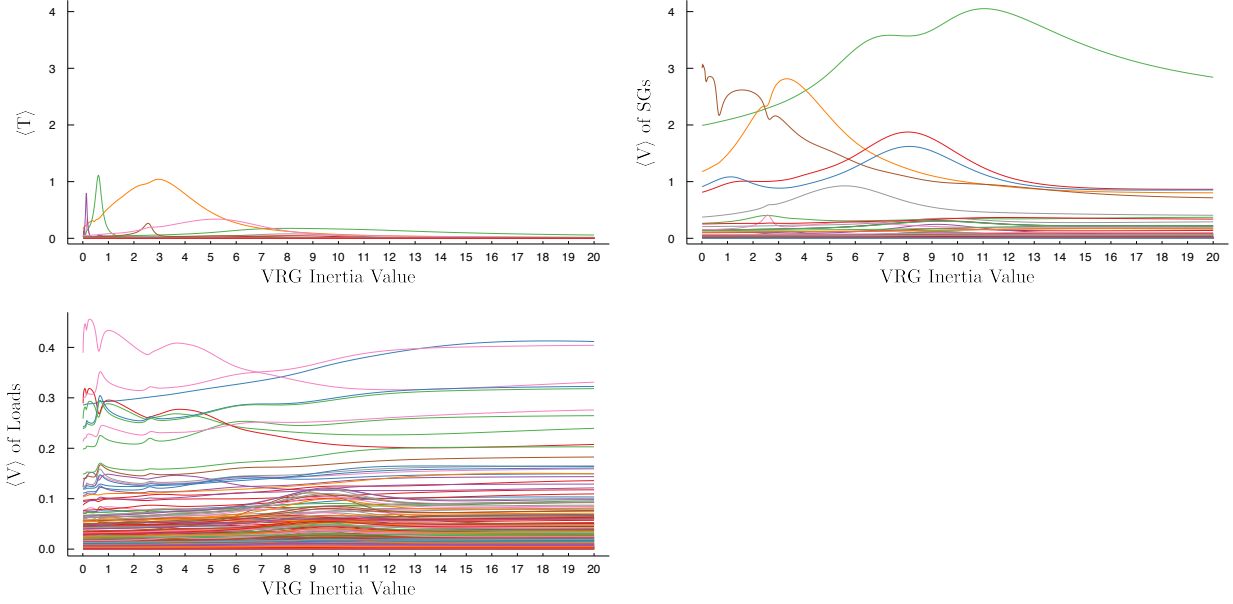


Figure 3.2: Example results for a single scenario (indicated in Figure 3.1) using the pulse perturbation. Each value is plotted as a function of the VRG inertia constant. *Top row:* The kinetic energy (left) and potential energy (right) of all SGs. *Bottom row:* The potential energy of all loads. Each colored trace indicates the response of a single component. SGs have the same colored trace in the kinetic and potential energy plots. The response of the components of the system are dependent on the VRG inertia value. Many of the traces have distinct maxima which are the primary feature characterized in this thesis.

potential energies. The top row of plots correspond to SGs where each SG has a different color. For example, the green trace in the top row of plots corresponds to the kinetic and nodal potential energy response of one SG as a function of the VRG inertia value. Similarly, the bottom plot of Figure 3.2 corresponds to the loads where each load is also distinguished by color.

Figure 3.2 clearly shows that the response of SGs and loads is highly dependent on the VRG inertia value. Specifically, many of the traces have distinct maxima. For example, consider the green and red traces in the nodal potential responses of SGs (top right plot of Figure 3.2) and the yellow and pink traces in the kinetic responses of SGs (top left plot). All of these traces have peaks, though they are at different inertia values and they have different magnitudes. The loads also have peaks in the nodal potential energy at different inertia values, and many of the traces have similar shapes. For example, the green and blue traces have a maximal response when the VRG

inertia value is large ($M_i \approx 18$), while the pink and red traces have peaks at a smaller inertia value ($M_i \approx 0.5$). In this thesis, I focus on analyzing the global maximum in the energetic responses of the SGs and loads. Although some of the traces also have local maxima (*i.e.* the green trace in the top right plot of Figure 3.2), it is important to first understand the mechanisms behind the global maximum, after which understanding the local maxima becomes straightforward. The next Section analyzes and discusses the global maxima of component energetic responses for all scenarios, and then relates these features to the concept of (de)localization.

3.2 Analysis of Global Maxima: All Scenarios

In this section I analyze and explain the relationship between the global maxima of the component energies and the VRG dynamical properties. The focus of this work is on understanding the (de)localization of power system dynamics and its relationship to a VRG inertia value and network location. Since (de)localization depends on the number and magnitude of component responses, a clear explanation of the dependence of component responses on the VRG dynamical properties is necessary. I specifically focus on characterizing the VRG inertia values and magnitudes of the global maxima.¹ The analyses that follow characterize these aspects of the maxima for *all* scenarios using the impulse perturbation.

The VRG inertia value that a global maximum occurs at is due to a resonance phenomenon as it depends on the natural (coupling) frequencies of the VRG and SGs/loads.² Consider two generators with an electrical distance of F_{ij} (see Section 2.1.2). The natural frequency of generator i as seen by generator j is defined as $\sqrt{\frac{F_{ij}}{M_i}}$ [citation]. Figure 3.3 plots the magnitude of the maximum response for the kinetic (left) and nodal potential (right) energies as a function of the ratio of the SG/load natural frequency to the VRG natural frequency. So, for example, if the global maximum occurs at the inertia value M_{peak} then the ratio is defined as $\frac{\sqrt{F_{i,VRG}/M_i}}{\sqrt{F_{VRG,i}/M_{peak}}}$. In Figure 3.3, peaks

¹ The width of the peaks are also descriptive of the oscillatory behavior, specifically it characterizes the damping ratio of the oscillations [citations]. I do not focus on this aspect of the oscillatory behavior in this work.

² Other work may refer to the natural frequency as the speed an oscillator would have if it was not connected to any other components. In this model that would be equal to the power production/consumption of the oscillator. However, I use the term natural frequency to refer to the coupling frequency between the oscillator and its neighbor(s).

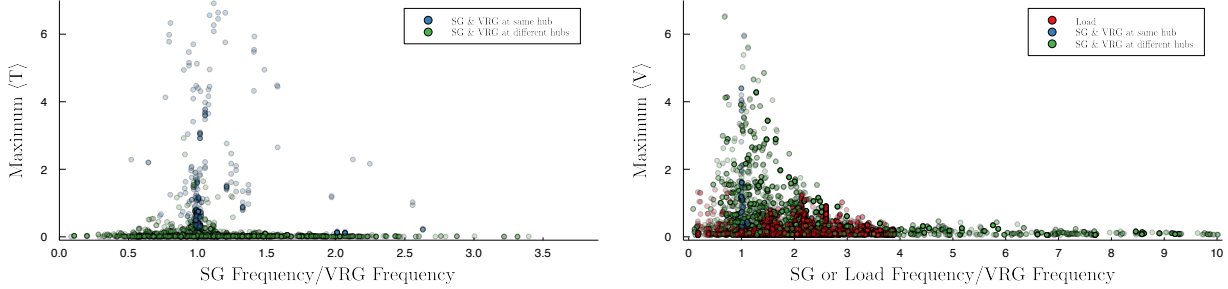


Figure 3.3: *Left:* Maximum kinetic energy response of an SG as a function of the ratio of the natural frequency of the SG and the VRG for each scenario. *Right:* Maximum potential energy response of a node as a function of the natural frequency ratio for each scenario. Each point corresponds to one peak value in one scenario, and all peaks are plotted for every scenario. The color of the point indicates the component type: blue points are SGs with the same neighbor as the VRG, green points are SGs that do not have the same neighbor as the VRG, and red points are loads. Statistics for these distributions are shown in Table 3.1.

associated with SGs are denoted by either blue or green points, where a blue point indicates the SG and VRG have the same neighbor while a green point indicates the SG and VRG do not have the same neighbor (I also refer to this as being at the same hub or not). Peaks associated with loads are denoted by red points. Informative statistics of these distributions are shown in Table 3.1. In general, Figure 3.3 illustrates, and Table 3.1 confirms, that larger values of $\langle T \rangle$ tend to occur closer to a ratio of one, regardless of whether the SG has the same neighbor as the VRG. On the other hand, the relationship between $\langle V \rangle$ and the frequency ratio appears to depend on the component. For SGs at the same hub as the VRG the ratio is still very close to one, but loads and SGs at a different hub than the VRG tend to have a ratio in the approximate range of 2 – 2.5. This indicates that SGs at the same hub as the VRG respond maximally in $\langle T \rangle$ and $\langle V \rangle$ at approximately the same natural frequency, while SGs at a different hub than the VRG respond at a different natural frequency for each energy type. Furthermore, SGs at a different hub than the VRG also tend to have higher magnitudes of $\langle V \rangle$ than $\langle T \rangle$, as opposed to SGs at the same hub where the magnitudes are comparable.

These results have a number of implications. First, it suggests that attempts to dampen oscillations, by say a power system stabilizer (PSS), between a VRG and SG at the same hub is

Table 3.1: Statistics of the natural frequency ratios and magnitudes shown in Figure 3.3. The statistics are broken down by component type.

Attributes of Peak	Component(s)	Mean	Median	Std. Dev.
Frequency Ratio, $\langle T \rangle$	SGs at same hub	1.138	1.006	0.353
	SGs at different hub	1.189	1.075	0.523
	All SGs	1.179	1.0356	0.497
Frequency Ratio, $\langle V \rangle$	SGs at same hub	1.040	1.005	0.080
	SGs at different hub	2.651	1.841	2.227
	All SGs	2.579	1.741	2.202
	Loads	2.096	2.133	0.707
Magnitude of $\langle T \rangle$	SGs at same hub	1.455	0.756	1.597
	SGs not at same hub	0.074	0.020	0.199
	All SGs	0.327	0.031	0.884
Magnitude of $\langle V \rangle$	SGs at same hub	1.158	0.747	1.33
	SGs not at same hub	0.615	0.267	0.831
	All SGs	0.639	0.277	0.866
	Loads	0.201	0.136	0.176

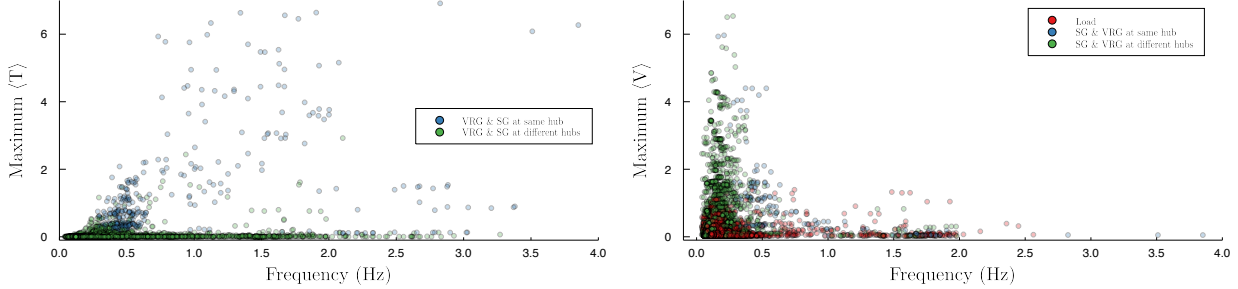


Figure 3.4: *Left:* Maximum kinetic energy response of each SG as a function of the VRG frequency. *Right:* Maximum nodal potential energy of the SGs and loads as a function of the VRG frequency for each scenario. Each point corresponds to one peak value in one scenario, and all peaks are plotted for every scenario. The color of the point indicates the component type: blue points are SGs with the same neighbor as the VRG, green points are SGs that do not have the same neighbor as the VRG, and red points are loads. Statistics for these distributions are shown in Table 3.2.

simpler because there is one dominant frequency for which both $\langle T \rangle$ and $\langle V \rangle$ respond maximally (and indeed PSS's are often used for these cases [citations]). However, dampening oscillations between a VRG and SG at different hubs is not as simple because there are two frequencies for which energy exchanges occur. Finally, these results suggest (though do not definitively show) that when the inertia value of the VRG is larger the potential energy tends to oscillate more in response to VRG fluctuations than the kinetic energy. Thus, the natural stored kinetic energy in SGs is not being used to help balance the system power. In order to verify that this is the case I examine the relationship between the magnitudes of the energy peaks and the frequency of the VRG.

As is clear from the variation of the heights of the points in Figure 3.3, the magnitude of the peaks depends on something other than matching frequencies. Specifically, the peak heights vary according to the frequency of the VRG. Figure 3.4 plots the magnitude of the $\langle T \rangle$ (left) and $\langle V \rangle$ (right) peaks versus the VRG frequency where they occur. Again, SGs are colored in either green or blue depending on if they are at the same hub as the VRG, while loads are red. The relevant statistics for these distributions are shown in Table 3.2.

The left plot of Figure 3.4 shows that SGs with the same neighbor as the VRG tend to have larger peaks and larger frequencies than SGs that do not have the same neighbor as the VRG. Table 3.2 indicates that SGs at the same hub as the VRG tend to have a frequency in the range of $0.5 - 1.5$

Table 3.2: Statistics of the frequencies of the global maxima for each energy type. The statistics are broken down by component type. These results relate to the pulse perturbation.

Attributes of Peak	Component(s)	Mean	Median	Std. Dev.
Frequency of $\langle T \rangle$	SGs at same hub	0.949	0.548	0.760
	SGs at different hub	0.347	0.207	0.403
	All SGs	0.388	0.221	0.462
Frequency of $\langle V \rangle$	SGs at same hub	0.793	0.519	0.621
	SGs at different hub	0.199	0.149	0.205
	All SGs	0.214	0.152	0.265
	Loads	0.188	0.159	0.179

Hz, which is consistent with operator experience with these types of oscillations [citations]. As the VRG frequency becomes smaller (inertia becomes larger), the magnitude of kinetic energy peaks become smaller as these peaks tend to be associated with SGs at a different hub than the VRG. The reason this occurs is that F_{ij} is *larger* for SGs at the same hub as the VRG than for SGs at a different hub, thus the frequency of peaks for SGs at the same hub is also larger (larger F_{ij} indicates that i and j are closer, see Section 2.1.2). Additionally, while the kinetic energy decreases at small frequencies, the potential energy has larger peaks at smaller frequencies. Table 3.2 shows that peaks in $\langle V \rangle$ tend to have smaller frequencies (in the approximate range of 0.2 – 1.0 Hz, depending on the component) than peaks in $\langle T \rangle$. This confirms the conjecture made previously that as the VRG inertia value becomes larger the VRG fluctuations tend to cause the potential energy to fluctuate more than the kinetic energy. Thus at larger inertia values most of the oscillations are observed in the angle state variables, which is directly related to the power generation/consumption of the component. The potential energy response is then the main energy stabilizer in the system instead of the naturally stored kinetic energy in the SGs, which is usually the preferred response [citations]. Furthermore, Table 3.2 indicates that the mean frequency of $\langle V \rangle$ for SGs (0.214 Hz) is larger than that of the loads (0.188 Hz), which further suggests that as inertia increases loads tend to oscillate more in response to VRG fluctuations, rather than the SGs. This highlights the known risk of oscillations that occur at small frequencies, and provides further evidence of the importance

of loads in small-signal stability [citations]. Specifically, this indicates that the ability of loads to dampen these oscillations is a key determinant in system stability [citation].

All of these results illustrate how and why individual components respond to VRG power fluctuations at different VRG inertia values. The VRG inertia value determines its natural frequency, which in turn impacts which components respond (SG or load, close or far), how they respond (kinetic or potential energy), and the magnitude of the response (how much the energy oscillates). At small VRG inertia values the kinetic energy is the primary response to power fluctuations, while at large inertia values the potential energy is the primary response. Furthermore, the kinetic responses (particularly for SGs at the same hub as the VRG) tend to be isolated, in that only a few components respond. On the other hand, the potential response (particularly those of the loads and SGs not at the same hub as the VRG) tends to include multiple components. This alludes to a transition from localized system dynamics (only a few components oscillating) to delocalized system dynamics (many components oscillating). This idea will be discussed further in Sections 3.4 and 3.5.

3.3 Impact of Perturbation Type

[WIP] Section 3.2 described the relationship between VRG dynamical properties and component responses for the impulse perturbation type. Although the impulse perturbation type is fairly representative of sudden and short power disturbances (*e.g.* faults), it is not realistic of the second to second power fluctuations that occur due to the variability of a renewable resource. Therefore, in this Section I perform a similar analysis as the previous, but for a stochastic perturbation which is representative of wind resource fluctuations (see Section 2.2.1 for perturbation details).

As an example of some of the dynamical differences between the impulse and stochastic perturbations, Figure 3.5 plots component energetic responses as a function of the VRG inertia value for a single scenario, the same scenario shown in Figure 3.2. The top row of plots in Figure 3.5 correspond to the kinetic (left) and potential (right) energy responses of SGs, while the bottom plot corresponds to the potential response of loads. In each plot, each individual component has a

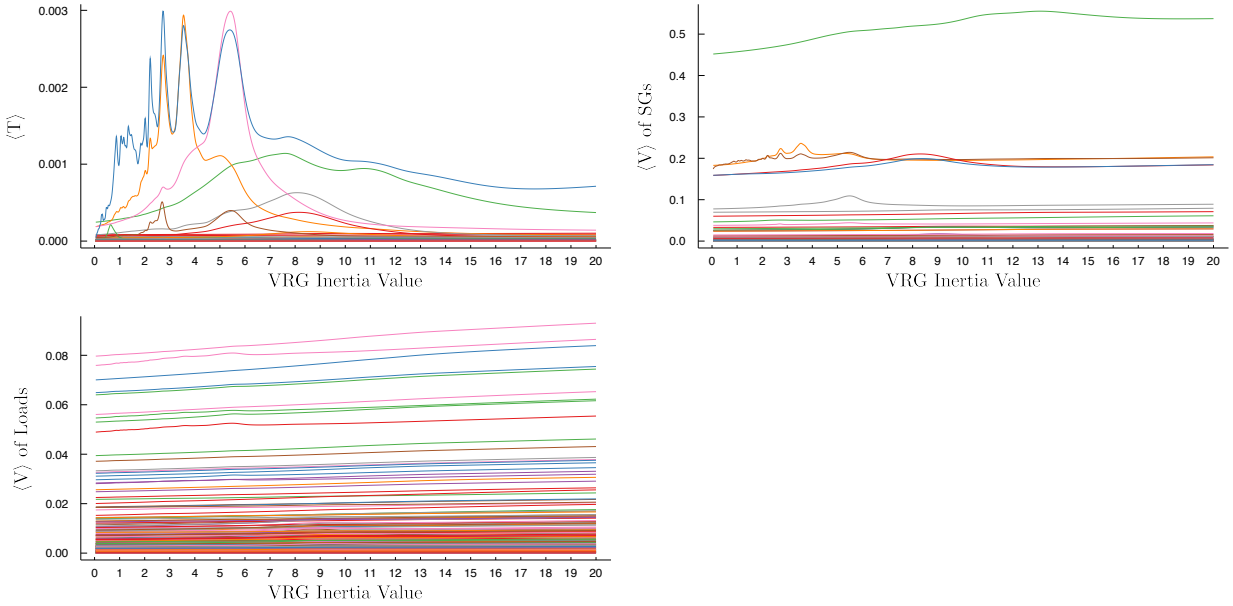


Figure 3.5: Example results for a single scenario (indicated in Figure 3.1) using the stochastic perturbation. Each value is plotted as a function of the VRG inertia constant. *Top row:* The kinetic energy (left) and potential energy (right) of all SGs. *Bottom row:* The potential energy of all loads. Each colored trace indicates the response of a single component. SGs have the same colored trace in the kinetic and potential energy plots. Components have the same colored trace as in Figure 3.2.

different color trace. Each component has the same colored trace in Figures 3.2 and 3.5 (*i.e.* the green trace in the top right plot of Figure 3.5 is the same component as the green trace in the top right plot of Figure 3.2).

There are a number of differences in the energetic responses of the components between the impulse and stochastic perturbation. Perhaps the biggest difference is in the magnitude of the responses. The energetic responses to the stochastic perturbation are significantly smaller than the impulse perturbation. Intuitively this makes sense as the magnitude of the stochastic fluctuations are smaller than the impulse perturbation, thus the responses to the stochastic perturbation are smaller (the largest stochastic disturbance is 5.43 and the mean disturbance is 0.595 while the impulse perturbation is $\Delta = 10.0$). Additionally, some of the traces in Figure 3.5 have numerous peaks whereas in Figure 3.2 they only have one (*e.g.* the yellow trace in the top left plots). The reason this is occurring is that the stochastic perturbation is continuously disturbing the VRG

power at a frequency that induces resonances that the pulse perturbation cannot induce [citation]. This is similar to perturbing a damped pendulum once (impulse) versus using a continuous driving force. Resonance is not possible for the impulse perturbation but it is possible with the continuous driving force [citation]. The differences observed between the impulse and stochastic perturbations for this single scenario can be observed in all of the other scenarios.

In order to offer a complete comparison of the component responses due to an impulse or stochastic perturbation for all scenarios, Tables 3.3 and 3.4 provide the same statistics for the stochastic perturbation as Tables 3.1 and 3.2 for the impulse perturbation. For further comparison, but to avoid too much redundancy, plots of the magnitude of the energy peaks as a function of the frequency ratio as well as the frequency can be found in Appendix A (Figures A.1 and A.2).

In general, most of the trends observed for the impulse perturbation can also be observed for the stochastic perturbation. For example, the dependence of the energetic responses on the VRG frequency is consistent across perturbation types (*i.e.* kinetic peaks tend to be at higher frequencies than potential peaks, peaks associated with SGs at the same hub as the VRG have larger frequencies than SGs that are not at the same hub). However, the magnitudes of the frequencies are different. Specifically, the frequencies of the impulse peaks are always larger than the frequencies of the stochastic peaks (for the same component and the same scenario). Furthermore, the frequency ratio of kinetic energy peaks tend to be close to one, specifically for SGs at the same hub as the VRG. On the other hand, SGs at a different hub than the VRG the frequency ratio of the kinetic peaks tends to be closer to approximately 1.5. Additionally, the frequency ratios of the potential energy peaks of SGs is very different depending on the perturbation type, with the stochastic ratios approximately two or three times larger than the impulse ratios (this is likely to change as I fill in the other inertia values for the stochastic perturbation scenarios).

It is important to consider the dynamical differences between the impulse and stochastic perturbation types as it impacts the component responses. As a result, the perturbation type is also likely to impact the (de)localization of system dynamics. Both of these perturbation types are representative of different kinds of power disturbances that can occur in power systems, and so it

Table 3.3: Statistics of the ratio of natural frequencies and magnitude of the global maxima for each energy type. The statistics are broken down by component type. These results relate to the stochastic perturbation.

Attributes of Peak	Component(s)	Mean	Median	Std. Dev.
Frequency ratio, $\langle T \rangle$	SGs at same hub	1.2823	1.037	0.861
	SGs at different hub	1.773	1.689	0.784
	All SGs	1.715	1.547	0.809
Frequency ratio, $\langle V \rangle$	SGs at same hub	6.951	3.514	7.855
	SGs at different hub	4.045	2.482	3.780
	All SGs	4.153	2.496	4.043
	Loads	1.876	1.810	0.548
Magnitude of $\langle T \rangle$	SGs at same hub	6.797×10^{-4}	4.820×10^{-4}	6.650×10^{-4}
	SGs at different hub	2.057×10^{-4}	9.432×10^{-5}	4.215×10^{-4}
	All SGs	2.619×10^{-4}	1.068×10^{-4}	4.820×10^{-4}
Magnitude of $\langle V \rangle$	SGs at same hub	0.137	0.089	0.181
	SGs at different hub	0.069	0.027	0.116
	All SGs	0.071	0.028	0.119
	Loads	0.021	0.012	0.027

Table 3.4: Statistics of the frequencies of the global maxima for each energy type. The statistics are broken down by component type. These results relate to the stochastic perturbation.

Attributes of Peak	Component(s)	Mean	Median	Std. Dev.
Frequency of $\langle T \rangle$	SGs at same hub	0.472	0.450	0.347
	SGs at different hub	0.127	0.096	0.116
	All SGs	0.141	0.099	0.149
Frequency of $\langle V \rangle$	SGs at same hub	0.162	0.141	0.087
	SGs at different hub	0.136	0.114	0.090
	All SGs	0.137	0.115	0.090
	Loads	0.132	0.121	0.056

is important to compare how each impacts the (de)localization of the system dynamics.

3.4 Quantifying the Delocalization Transition

As Section 3.2 briefly suggests, there is a possible transition in the system dynamics where at small inertia values only a few components respond (localized dynamics) whereas at large inertia values many components respond (delocalized dynamics). In order to better understand this possible transition, I use the inverse participation ratio (IPR) of the system dynamics to quantify the degree of (de)localization (see Section 2.1.2.1). Specifically, let $\hat{\mathbf{x}} = [\langle \omega_1 \rangle, \langle \omega_2 \rangle, \dots, \langle \delta_{n-1} \rangle, \langle \delta_n \rangle]$ be a normalized vector where $\langle \rangle$ indicates the RMS of the state variable (measured from its steady-state value) for a given simulation. I compute $\text{IPR}(\hat{\mathbf{x}}) = \sum_{i=1}^n x_i^4$ which quantifies the number of state variables that oscillated significantly for a given simulation. If $\text{IPR}(\hat{\mathbf{x}}) = 1$ then only one state variable oscillated significantly during the simulation (completely localized dynamics), whereas a value of $\text{IPR}(\hat{\mathbf{x}}) = \frac{1}{n}$ indicates that every state variable oscillated during the simulation (complete delocalization).

As an example, Figure 3.6 plots $\text{IPR}(\hat{\mathbf{x}})$ as a function of the VRG inertia constant for the same scenario discussed in Sections 3.1 and 3.3. The red trace refers to the pulse perturbation while the blue trace refers to the stochastic perturbation. The two points correspond to the final local maxima that occurs in the system IPR, and will be discussed later on in this Section.

Figure 3.6 shows that both perturbation types are more localized at small inertia values and more delocalized at large inertia values. However, the dynamics due to a pulse perturbation are more localized than the dynamics due to a stochastic perturbation at all inertia values, where the most extreme differences occur at smaller inertia values. This can likely be contributed to differences in magnitudes of the two perturbations. The magnitudes of the stochastic perturbations are much smaller than the pulse perturbations which means that the perturbation frequency will also be smaller. In terms of the system Jacobian, this means that eigenvectors with smaller eigenvalues are excited, and almost all nodes participate in this motion [citation] (see Section 2.1.1). On the other hand, the pulse perturbation will have larger perturbation frequencies than the stochastic

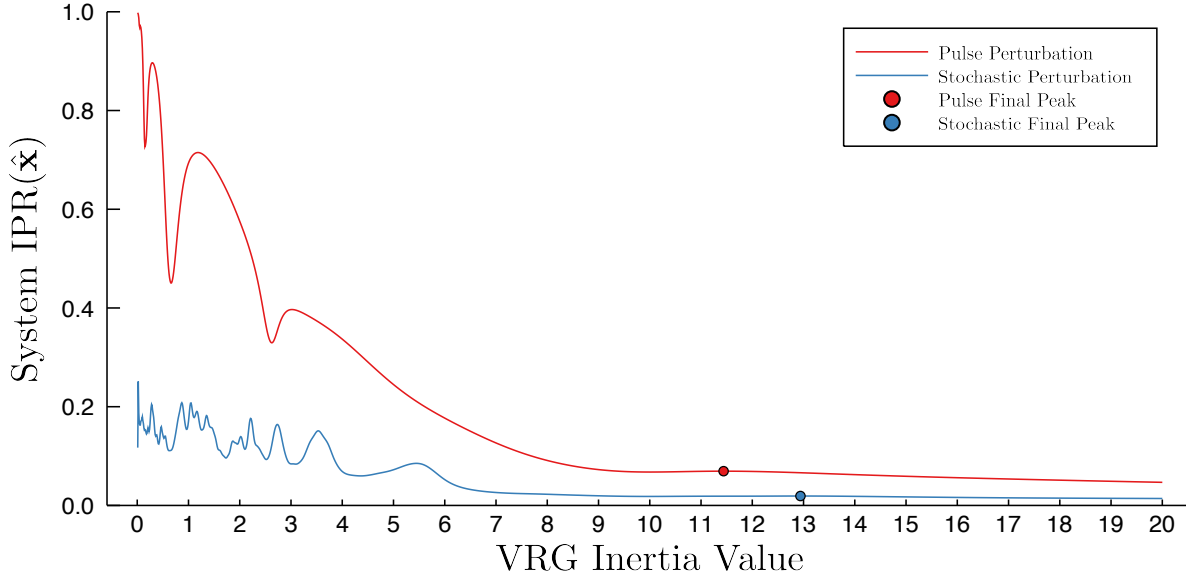


Figure 3.6: IPR of the system dynamics for the example scenario shown in Figure 3.1. The red trace refers to the pulse perturbation and the blue trace refers to the stochastic perturbation. The corresponding colored points indicate the final local maxima of these traces.

perturbation, which means that the excited eigenvectors are more localized [citation]. Thus, in this work, $\text{IPR}(\hat{\mathbf{x}})$ due to the stochastic perturbation is always more delocalized than $\text{IPR}(\hat{\mathbf{x}})$ due to the pulse perturbation, for all scenarios.

Although $\text{IPR}(\hat{\mathbf{x}})$ decreases as inertia increases for both perturbation types, it is not a monotonic decrease, as a number of local extrema can be observed in both traces in Figure 3.6. In general, the local maxima tend to correspond with the peaks in $\langle T \rangle$ and $\langle V \rangle$. To show this, Figure 3.7 has four marginal histograms for the differences in the peaks of $\text{IPR}(\hat{\mathbf{x}})$ with the peaks of $\langle T \rangle$ (left plots) and $\langle V \rangle$ (right plots). The top row of plots correspond to the results from the pulse perturbation and the bottom row of plots correspond to the results from the stochastic perturbation. The horizontal axis for each plot indicates the difference in the inertia values of peaks in the energies and the closest peak of $\text{IPR}(\hat{\mathbf{x}})$. In other words, for each peak in $\langle T \rangle$ and $\langle V \rangle$ I find the closest peak in $\text{IPR}(\hat{\mathbf{x}})$ and compute the difference in inertia values for the two. The color of each square in Figure 3.7 corresponds to the number of points that are within that square, where

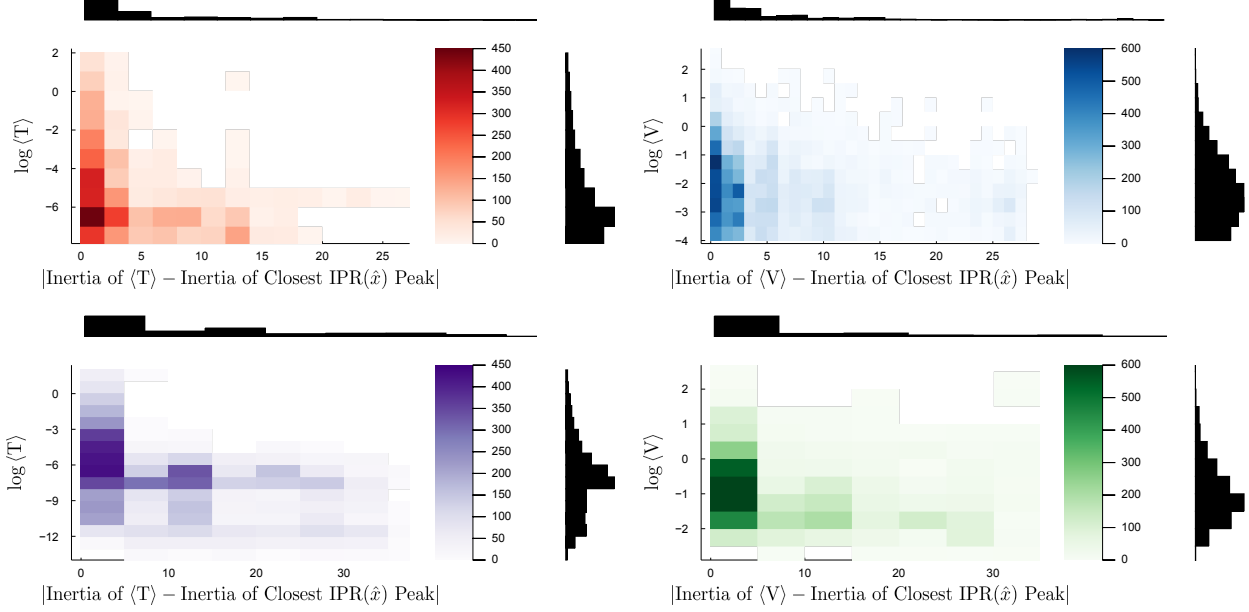


Figure 3.7: Each of these marginal histograms shows the relationship between the size of the energy peak and the difference in inertia between that peak and the closest peak in the system IPR trace. The top row of plots correspond to the pulse perturbation while the bottom row of plots correspond to the stochastic perturbation. The left column of plots correspond to the kinetic energy and the right column of plots correspond to the potential energy.

a darker color indicates more points within that square.

In general, peaks in $\langle T \rangle$ tend to correspond to peaks in $\text{IPR}(\hat{x})$, for both perturbation types. This is indicated by the fact that darker squares tend to be at smaller inertia differences in the two left most plots of Figure 3.7. Although the darkest square for the stochastic perturbation type (bottom left plot) occurs at a much larger inertia value (approximately between 15 – 20), the magnitude of the peaks that fall within this square are quite small as compared to those peaks that have a smaller inertia difference.

Peaks in $\langle V \rangle$ can be close to a peak in $\text{IPR}(\hat{x})$, but there are also many peaks that are not close to a peak in $\text{IPR}(\hat{x})$. These two cases correspond to the trends illustrated in Section 3.2. Specifically, peaks in $\langle V \rangle$ with a small inertia difference to a peak in $\text{IPR}(\hat{x})$ likely correspond to an SG at the same hub as the VRG. This is due to the fact that SGs at the same hub as the VRG tend to have peaks in $\langle T \rangle$ and $\langle V \rangle$ at approximately the same VRG inertia value. Thus, if the peak

in $\langle T \rangle$ is close to a peak in $\text{IPR}(\hat{\mathbf{x}})$, then the peak in $\langle V \rangle$ will also be close to a peak in $\text{IPR}(\hat{\mathbf{x}})$. For peaks in $\langle V \rangle$ that are not close to a peak in $\text{IPR}(\hat{\mathbf{x}})$, this indicates that there are likely many peaks in $\langle V \rangle$ that occur at the same value. If the peak in $\langle V \rangle$ was isolated (*i.e.* no other components responding) then we would expect $\text{IPR}(\hat{\mathbf{x}})$ to increase. As an example, consider all of the traces in the bottom left plot of Figure 3.2 that have the same shape. The peak values for each of those traces occur at roughly the same inertia value.

These results show that $\text{IPR}(\hat{\mathbf{x}})$ can indeed quantify the degree to which the system dynamics are (de)localized. Specifically, the local maxima in $\text{IPR}(\hat{\mathbf{x}})$ can be associated with peaks in $\langle T \rangle$ and some of the peaks in $\langle V \rangle$, for both perturbation types. Using this fact, I define the delocalization transition point as the final peak of $\text{IPR}(\hat{\mathbf{x}})$. As an example, these peaks are denoted by the red and blue points in Figure 3.6. Let the inertia value where this final peak occurs be denoted by M^* . For each scenario, I use M^* as the separation between localized oscillatory behavior and delocalized behavior. The last peak in the system IPR is the final instance of the system oscillatory behavior becoming more localized, after which the dynamics only become more delocalized. Choosing a transition point $M < M^*$ would put the final instance of (relatively) localized dynamics in the regime of delocalized dynamics, and vice-versa for $M > M^*$. However, the value of M^* is not enough to quantify the delocalization transition as it does not indicate anything about how (de)localized the oscillations are for $M \geq M^*$. In order to take into account the (de)localization at M^* and the rate of delocalization for $M > M^*$, I use the integral of the system IPR from M^* to the final (tested) inertia value. I refer to this integral as the delocalization transition.

The delocalization transition indicates how much oscillations spread from the VRG to other nodes in the network. A large delocalization transition indicates that oscillations spread to only a few nodes, while a small delocalization transition indicates that oscillations spread to many nodes. Although it may seem that a larger delocalization transition is preferable to a smaller one because less nodes are impacted by the fluctuations, this may not always be the case. A large delocalization transition not only indicates that oscillations spread less, but it also indicates that less nodes help stabilize the system due to the fluctuations. Rather than spread the oscillatory energy among many

nodes such that each only oscillates a little, the oscillations are spread among less nodes that will oscillate more. Whether or not this is beneficial to system stability is highly dependent on the power system (*i.e.* whether or not the fluctuating components stay in a valid operating range). Regardless of what constitutes a desirable delocalization transition, it is important to understand how it depends on the network structure and the VRG inertia value.

3.5 Measuring Node Structural Similarity

Having quantified the delocalization transition for each scenario, I will now examine the measure I use in this work to quantify the ability of a node to spread oscillations throughout the network. I use the concept of dynamic sensitivity to connect the delocalization transition with the network structure. Recall from Section [blah] that the dynamic sensitivity of a node quantifies how much a node responds to perturbations, such that a larger dynamic sensitivity indicates a stronger response to perturbations. Specifically, the dynamic sensitivity of node i is defined as $s_i = \sum_{k=2}^n \frac{|v_i^k|}{\lambda_k}$ where v_i^k refers to the i^{th} entry of the k^{th} eigenvector of the network Laplacian. I define the *sensitivity vector* as the vector that contains the addends of the dynamic sensitivity sequence: $\hat{s}_i = [\frac{|v_i^2|}{\lambda_2}, \frac{|v_i^3|}{\lambda_3}, \dots, \frac{|v_i^{n-1}|}{\lambda_{n-1}}, \frac{|v_i^n|}{\lambda_n}]$. Each entry in the sensitivity vector defines the response of the node for each fundamental motion of the system.³ Before exploring the relationship between sensitivity vectors and the delocalization transition, I explain how the sensitivity vector can describe the ability of a node to spread oscillations. I then outline some features of the sensitivity vectors for a random graph model with known structural and dynamical characteristics.

The more similar the fundamental motions of two nodes are the more likely it is that a random perturbation of one node will induce a response in the other. Consider a graph with two pendant nodes that share a neighbor and have equivalent dynamical parameters (similar to the exact localization example discussed in Section [blah]). Due to the graph and parameter symmetry, these nodes will have the same (absolute) entries in every eigenvector. Thus perturbing one of these

³ See Section [blah] for an explanation of the equivalence of the eigenvectors of the network Laplacian and the eigenvectors of the system Jacobian.

nodes will always induce a response in the other. Now consider the third node in this graph, the shared neighbor of the two pendant nodes. There is only one (non-trivial) eigenvector for which the third node has a non-zero value and it describes the motion where the two pendant nodes are oscillating in-phase with each other but anti-phase with the third node (*i.e.* the eigenvector has the form $[x, x, -2x]$). In order for oscillations to spread from the pendant nodes to the third node (or vice-versa) this fundamental mode must be excited. On the other hand, exciting any of the fundamental modes will cause the two pendant nodes to oscillate. This indicates that the two pendant nodes are more dynamically similar to each other than the third node. A random perturbation of one of the pendant nodes is more likely to spread to the other pendant node than it is to the third node.

I quantify this notion of similarity presented above by measuring the angle between the sensitivity vectors of two nodes. In the example, the angle between the sensitivity vectors of the two pendant nodes is zero because the vectors are equivalent. On the other hand, the angle between the third node and either of the two pendant nodes is approximately $\pi/18$. This reflects the dynamical difference between the third node and the other two nodes. In the rest of this work, I refer to the angle between the sensitivity vectors of node i and node j as α_{ij} and $\boldsymbol{\alpha}_i$ to refer to the set of angles between node i and all other nodes in the network.

Before exploring how $\boldsymbol{\alpha}_i$ is related to the delocalization transition, I first want to explain what $\boldsymbol{\alpha}_i$ looks like for small-world (SW) random graphs. Power grids have many similarities with SW random graphs [citations]. Thus, understanding how $\boldsymbol{\alpha}_i$ depends on the parameters of SW graphs will provide insight into how $\boldsymbol{\alpha}_i$ may describe some of the dynamical properties of power grids.

SW random graphs with n nodes are generated by first creating a ring network where each node is connected to its k nearest neighbors on the ring, and then each edge is rewired with a probability of p where the new nodes to be connected are chosen uniformly at random. When the value of p is large the graph approaches a random graph similar to the Erdos-Renyi random graph, and when p is small it more closely resembles the original ring graph [citation]. I generate SW graphs of size $n = 100$ and $k = 4$ with probabilities in the range $0.05 - 0.95$ with a step of 0.05 .⁴

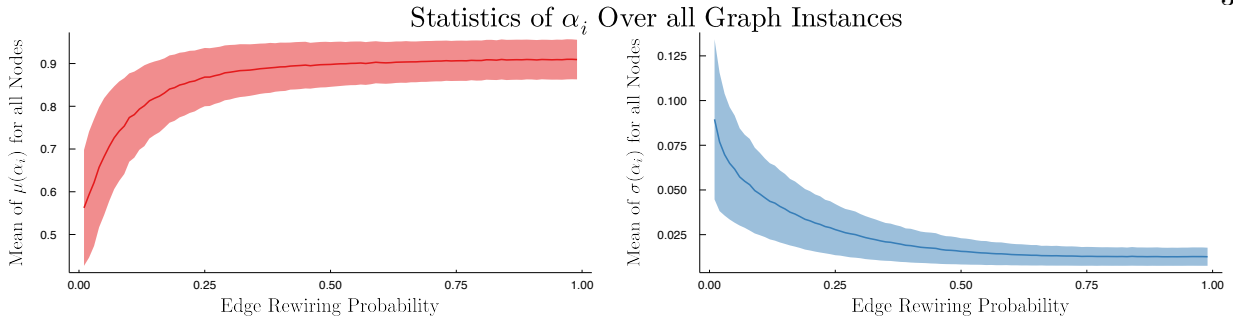


Figure 3.8: Statistics of α_i for 1000 different SW graphs with $n = 100$ and $k = 4$. *Left:* The mean of $\mu(\alpha_i)$ averaged over all graphs. *Right:* The mean of $\sigma(\alpha_i)$ averaged over all graphs. The shaded regions indicate the standard deviation of $\mu(\alpha_i)$ and $\sigma(\alpha_i)$. As the randomness of the graph increases, the mean value of $\mu(\alpha_i)$ increases while $\sigma(\alpha_i)$ decreases which indicates that angles become more orthogonal and less varied.

For each probability value, I generate 1000 different SW graphs. For each SW graph generated, I compute the mean of α_i ($\mu(\alpha_i)$) and variance of α_i ($\sigma(\alpha_i)$) for each node in the network. I then compute the mean and standard deviation of $\mu(\alpha_i)$ and $\sigma(\alpha_i)$ for all nodes in all of the graphs associated with probability p .

Figure 3.8 plots the mean of $\mu(\alpha_i)$ (left) and $\sigma(\alpha_i)$ (right) as a function of p . The mean is indicated by the dark trace and the shaded regions indicate the standard deviation of the values at that point. As the probability of edge rewiring increases $\mu(\alpha_i)$ increases, while $\sigma(\alpha_i)$ decreases. This indicates that the more random a graph is the more orthogonal the nodes' sensitivity vectors are and the less variation there is in the distribution of α_i . Furthermore, the largest changes in $\mu(\alpha_i)$ and $\sigma(\alpha_i)$ occur at small probability values, approximately in the range $p = .05 - 0.25$. This suggests that α_i has the most variation among nodes when the graph is less random and more ring-like.

To better understand how α_i depends on where a node is in the network, Figures 3.9 and 3.10 plot 2D histograms of $\mu(\alpha_i)$ and $\sigma(\alpha_i)$ versus the node's entry in the Fiedler vector of the network, for four different probability values. The color of each grid cell indicates the number of nodes in that cell, and all nodes from all graphs associated with that probability are included. Recall from

⁴ I tested multiple values of $k = 4, 6, 8$ but there were no significant differences.

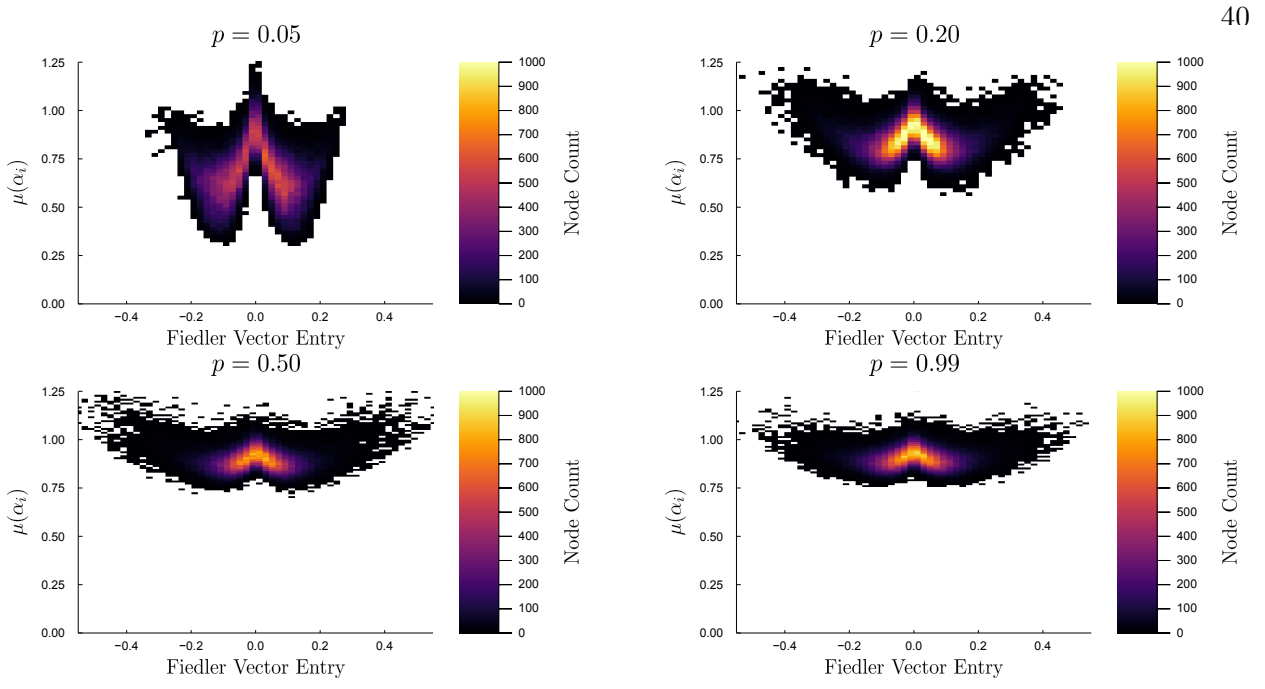


Figure 3.9: 2D histograms of $\mu(\alpha_i)$ versus node i 's Fiedler vector entry for four different probabilities of 1000 different SW random graphs. The color of each cell indicates the number of nodes within the cell. For small probabilities, a v-shape is present with high values of $\mu(\alpha_i)$ occurring mostly in the center of the network (Fiedler entries close to zero) and with smaller values of $\mu(\alpha_i)$ occurring towards the outside of the network (most positive or most negative Fiedler vector entries). As the probability increases, the v-shape flattens and less variability in $\mu(\alpha_i)$ is observed for different parts of the network.

Section 2.1.2 that the Fiedler vector bisects a graph such that nodes with more positive/negative entries are closer to the outside of the network and nodes with entries closer to zero are more towards the center of the network [citations]. For small probabilities, $\mu(\alpha_i)$ has a clear dependence on the network structure. Specifically, high values of $\mu(\alpha_i)$ tend to occur towards the center of the network while smaller values tend to occur towards the outside of the network. As the probability increases the v-shape shown in the top left plot of Figure 3.9 flattens out and much less variability is observed in $\mu(\alpha_i)$. This confirms that as the randomness of a graph increases the sensitivity vectors of the nodes become more orthogonal, regardless of where they are located in the network. A similar phenomenon is observed for the variability of α_i . The top left plot of Figure 3.10 exhibits a wide range of values and appears to have only a slight w-shape. As the probability increases the w-shape flattens, with the most noticeable w-shape occurring at intermediate probabilities such

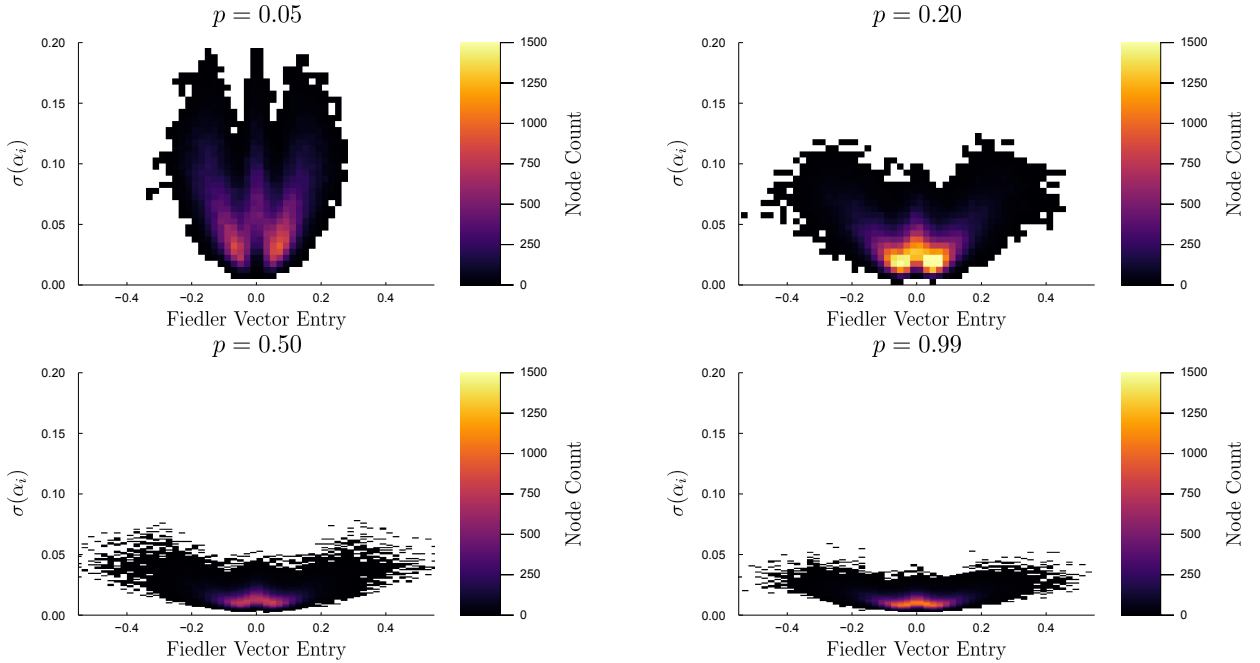


Figure 3.10: 2D histograms of $\sigma(\alpha_i)$ versus node i 's Fiedler vector entry for four different probabilities of 1000 different SW random graphs. The color of each cell indicates the number of nodes within the cell. For small probabilities, $\sigma(\alpha_i)$ appears to have a circular structure, which flattens into a more parabolic structure as the probability increases. The smallest values tend to occur near the center of the network, while larger values of $\sigma(\alpha_i)$ are observed on the outsides of the network. This indicates that nodes that are close to the center of the network have less variability in α_i than nodes towards the outside of the network.

as $p = 0.20$. This confirms that the variability of the sensitivity vector angles decreases as the randomness of a graph increases.

These results suggest that $\mu(\alpha_i)$ and $\sigma(\alpha_i)$ are both descriptive of differences among the nodes in the network. Specifically, $\mu(\alpha_i)$ describes the average structural similarity of node i to the rest of the nodes, while $\sigma(\alpha_i)$ describes the variability of those similarities. Furthermore, because the sensitivity vector is also descriptive of the node's dynamics, $\mu(\alpha_i)$ and $\sigma(\alpha_i)$ not only describe structural similarity among the nodes, but they also describe dynamical similarities.

3.6 Dependence of Delocalization Transition on Network Structure

In Section 3.4 I described how the IPR of the system dynamics can be used to quantify the delocalization transition, and in Section 3.5 I illustrated and quantified the connection between the network structure and the network dynamics. In this Section, I directly compare the delocalization transition with the structural measure. Due to the fact that both the mean and the variance of α_i are important and descriptive, I compute the *dispersion index* of α_i which is defined as the variance divided by the mean.

Figure 3.6 plots the delocalization transition of each scenario as a function of its dispersion index. Each point is one scenario, and the red points indicate the results from the impulse perturbation while the blue points indicate the results from the stochastic perturbation. I computed a line of best fit for each perturbation type using the method of least squares. Each fit is shown as a colored dashed line with its equation and coefficient of determination written above the line.

Figure 3.6 shows a clear relationship between the delocalization transition and the dispersion index. In general, a smaller dispersion index indicates a larger delocalization transition. There are two ways the dispersion index can be small: the variance is small or the mean is large. Both of these have similar dynamical implications. A small variance indicates that, regardless of the mean, most of the nodes in the network have a similar response to perturbations of that VRG node. Thus, if the common dynamical mode(s) are not excited then most of the nodes will not respond to fluctuations at that VRG location, which makes it harder for oscillations to spread from

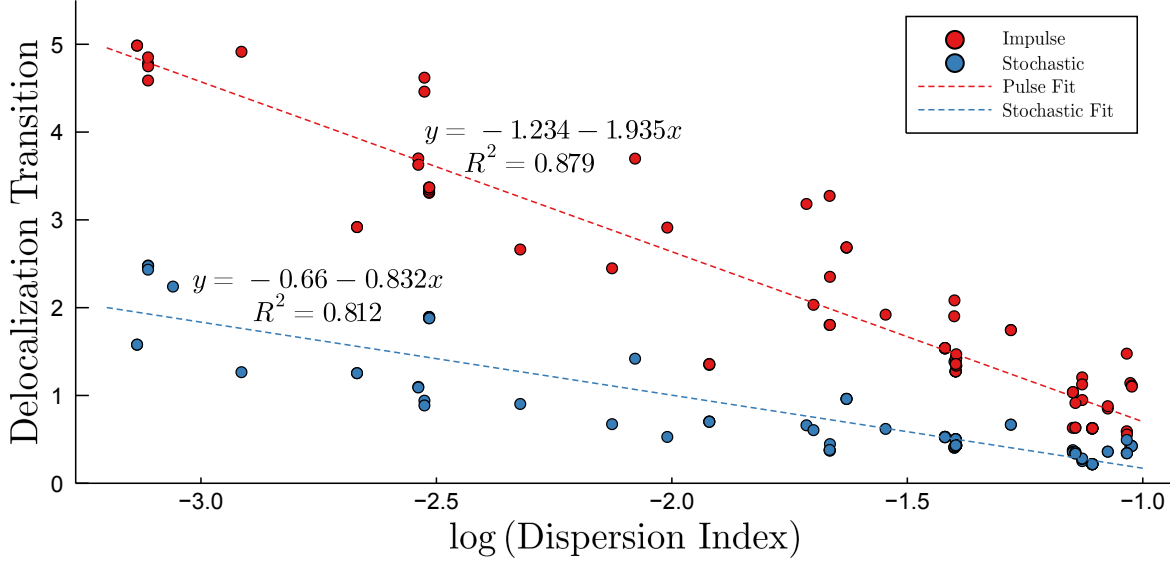


Figure 3.11: The delocalization transition as defined in Section 3.4 as a function of the dispersion index of α_i defined in Section 3.5. Each point corresponds to a single scenario and the color of the point indicates the perturbation type (red is the pulse, blue is the stochastic). Two lines of best fit are shown with their equations and coefficients of determination shown above the lines.

that location. Similarly, a large mean indicates that the VRG sensitivity vector is more orthogonal to the rest of the node's sensitivity vectors. This also means that there are only a few (possibly fewer than if the variance was small) common dynamical modes for which oscillations will spread from that VRG location. On the other hand, a larger dispersion index tends to indicate a smaller delocalization transition. The dispersion index can be large if the variance is large or the mean is small. If the variance is large, that means that the VRG has a number of dynamical modes that will excite various nodes, which makes it more likely that a random perturbation will induce a response from a node. If the mean is small, this means that the VRG's sensitivity vector is very similar to the sensitivity vectors of other nodes and so perturbations of the VRG will induce oscillations in more nodes.

The difference between the two perturbation types is particularly interesting. There is approximately a squared relationship for the impulse perturbation and approximately a linear relationship for the stochastic perturbation (the horizontal axis is a log scale). [I need to think more about

what this means and why it could be happening.]

3.7 Future Work

[WIP: This section is not complete. It is a place holder for some sentences which I like, but have not decided where to put.]

Future work will continue to explore the relationship between α_i and the dynamical characteristics of the nodes.

It is useful and important to know how specific network changes (such as strengthening a line, adding more components, or changing dynamical parameters) will impact the oscillatory dynamics without running (generally time consuming) simulations.